

Article

Synergistic Adsorption-Catalytic Sites TiN/Ta₂O₅ with Multidimensional Carbon Structure to Enable High-Performance Li-S Batteries

Chong Wang ¹, Jian-Hao Lu ², Zi-Long Wang ², An-Bang Wang ², Hao Zhang ², Wei-Kun Wang ^{2,*}, Zhao-Qing Jin ^{2,*} and Li-Zhen Fan ^{1,*} 

¹ Beijing Advanced Innovation Center for Materials Genome Engineering, Institute of Advanced Materials and Technology, University of Science and Technology Beijing, Beijing 100083, China; wangchong18810@163.com

² Military Power Sources Research and Development Center, Research Institute of Chemical Defense, Beijing 100191, China; hahalujianhao@163.com (J.-H.L.); wangzilong0709@163.com (Z.-L.W.); wab_wang2000@163.com (A.-B.W.); dr.h.zhang@hotmail.com (H.Z.)

* Correspondence: wangweikun2002@163.com (W.-K.W.); jinzhaoqing1001@gmail.com (Z.-Q.J.); fanlizhen@ustb.edu.cn (L.-Z.F.)



Citation: Wang, C.; Lu, J.-H.; Wang, Z.-L.; Wang, A.-B.; Zhang, H.; Wang, W.-K.; Jin, Z.-Q.; Fan, L.-Z. Synergistic Adsorption-Catalytic Sites TiN/Ta₂O₅ with Multidimensional Carbon Structure to Enable High-Performance Li-S Batteries. *Nanomaterials* **2021**, *11*, 2882. <https://doi.org/10.3390/nano11112882>

Academic Editor: Byungwoo Park

Received: 17 September 2021

Accepted: 23 October 2021

Published: 28 October 2021

Publisher's Note: MDPI stays neutral with regard to jurisdictional claims in published maps and institutional affiliations.



Copyright: © 2021 by the authors. Licensee MDPI, Basel, Switzerland. This article is an open access article distributed under the terms and conditions of the Creative Commons Attribution (CC BY) license (<https://creativecommons.org/licenses/by/4.0/>).

Abstract: Lithium-sulfur (Li-S) batteries are deemed to be one of the most optimal solutions for the next generation of high-energy-density and low-cost energy storage systems. However, the low volumetric energy density and short cycle life are a bottleneck for their commercial application. To achieve high energy density for lithium-sulfur batteries, the concept of synergistic adsorptive-catalytic sites is proposed. Base on this concept, the TiN@C/S/Ta₂O₅ sulfur electrode with about 90 wt% sulfur content is prepared. TiN contributes its high intrinsic electron conductivity to improve the redox reaction of polysulfides, while Ta₂O₅ provides strong adsorption capability toward lithium polysulfides (LiPSs). Moreover, the multidimensional carbon structure facilitates the infiltration of electrolytes and the motion of ions and electrons throughout the framework. As a result, the coin Li-S cells with TiN@C/S/Ta₂O₅ cathode exhibit superior cycle stability with a decent capacity retention of 56.1% over 300 cycles and low capacity fading rate of 0.192% per cycle at 0.5 C. Furthermore, the pouch cells at sulfur loading of 5.3 mg cm⁻² deliver a high areal capacity of 5.8 mAh cm⁻² at low electrolyte/sulfur ratio (E/S, 3.3 μL mg⁻¹), implying a high sulfur utilization even under high sulfur loading and lean electrolyte operation.

Keywords: lithium-sulfur batteries; catalyst; TiN/Ta₂O₅; multidimensional carbon

1. Introduction

Lithium-sulfur (Li-S) batteries are ideal candidates to substitute conventional lithium-ion batteries [1]. However, despite their attractive merits including high theoretical energy density and abundant resources, the practical uses of Li-S batteries are still hampered by a series of deleterious defects facing widespread commercialization, such as the intrinsic poor electrical conductivity of sulfur and discharge products (Li₂S/Li₂S₂), the shuttling phenomenon originated from the dissolution of lithium polysulfide (LiPSs), and, particularly, the sluggish conversion of LiPSs to solid lithium sulfides, bringing about low sulfur utilization, fast capacity fading, and poor cyclability [2].

Accordingly, strategies have been developed to solve the above problems in the past few decades. It has been corroborated that the conversion of LiPSs on the interface between the electrolyte and host materials is decided by their moderate interactions and fast electron/ion exchange [3]. Catalysts such as transition metal-free polar materials [4,5], transition metal compounds [6–9], and metals [10] can not only capture LiPSs to decrease their dissolution and diffusion in the electrolyte but also boost the conversion between LiPSs and Li₂S₂/Li₂S. Among them, titanium nitride has been widely used as the catalytic material [11,12], due to its high electrical conductivity, which can propel the kinetics of

the transformation of LiPSs. Goodenough and coworkers reported a mesoporous TiN with a high surface area, benefiting from its intrinsic electrical conductivity, fine porous framework, and appropriate adsorption ability of TiN; the TiN-S composite cathode exhibits high specific capacity and excellent rate capability [13]. However, TiN nanoparticles (TiN NPs) cannot effectively suppress the shuttle effects of LiPSs, because of their weak adsorption capacity toward LiPSs [14]. Kim et al. proposed an effective electrocatalyst Ta_2O_5 for LiPSs conversion in the Li-S system; the intrinsic chemical polarity of Ta_2O_5 could establish favorable interactions with the LiPSs [15]. However, Ta_2O_5 demonstrates insufficient electrical conductivity, because of its electron band structure [16], which does not provide desirable electron mobility and catalytic activity. Therefore, it is difficult to make full use of catalysis ability depending on the sole component, which is short in either adsorption or electrical conductivity. Especially with high sulfur loading for a thick cathode, the sluggish and incomplete conversion of LiPSs to solid lithium sulfides limits the full utilization of intermediates, leading to the shuttle effect and rapid capacity decay during cycling.

To attain high specific capacity under the condition of high sulfur content of the sulfur-based composite and thick sulfur cathode, we designed the $TiN@C/S/Ta_2O_5$ cathode for Li-S batteries. Both TiN and Ta_2O_5 have a synergy enhancement effect to promote the affinity with LiPSs and speed up the kinetics of sulfur conversion reaction. In addition, the multidimensional carbon structure, which is the mixture of Super P, CNT, and graphene, can offer high electrical conductivity and sustain the strain generated by the volumetric changes of the active materials during cycling [17]. Their characteristic superiorities endow our high fraction of sulfur cathode with good rate response capability and superior cyclability even under high sulfur loading and lean electrolyte/sulfur ration operation.

2. Experimental Section

2.1. Preparation of $TiN@C/S/Ta_2O_5$ Composite

The $TiN@C/S/Ta_2O_5$ composite was fabricated in a typical liquid-phase suspension process. A certain amount of Super P, CNT, graphene, and TiN NPs (the weight ratio of Super P: CNT: G: TiN = 2:2:1:10) was ball-milled to obtain the uniform slurry. Sulfur was synthesized based on the reaction between $Na_2S_2O_3$ and HCOOH [18]; the suspension of sulfur was injected into the mixed solution of $TiN@C$ under vigorous stirring for more than 10 h. After that, the sediment was obtained by filtering, washed with distilled water several times to wipe off the soluble impurities, and dried under vacuum 60 °C for 24 h. Next, the $TiN@C/S$ materials were uniformly dispersed in distilled water again, and an appropriate amount of $Ta(OEt)_5$ was added to the above suspension; the amorphous Ta_2O_5 was produced by the hydrolysis reactions between $Ta(OEt)_5$ and deionized (DI) water [19]. Subsequently, the mixture was stirred all night. Finally, the $TiN@C/S/Ta_2O_5$ (the weight ratio of Super P: CNT: G: TiN: Ta_2O_5 = 2:2:1:10:10) composite was collected by centrifugation, washed with deionized water several times, and dried at 60 °C for 24 h. The $TiN@C/S$ (SuperP: CNT: G: TiN = 2:2:1:20) and $Ta_2O_5@C/S$ (Super P: CNT: G: Ta_2O_5 = 2:2:1:20) composites were prepared with the procedure similar to $TiN@C/S/Ta_2O_5$ composite; the content of sulfur in both $TiN@C/S$ and $Ta_2O_5@C/S$ materials is also 90 wt%.

The sulfur composite cathodes were prepared by mixing the active material ($TiN@C/S/Ta_2O_5$), Super P, carbon nanotube, and a binder (LA133) in deionized water and isopropanol mixed solution with a weight ratio of 80:5:5:10. After stirring for 12 h, the cathode slurry was blade-cast onto Al foils, followed by drying at 60 °C for 24 h. Similarly, the $TiN@C/S$ and $Ta_2O_5@C/S$ composites were prepared.

2.2. Material Characterization Techniques

Thermogravimetric analysis (NETZSCH TG 209F3, NETZSCH Gerätebau GmbH, Selb, Germany) was carried out with a heating rate of 5 °C min⁻¹ under an atmosphere of N_2 . The metallic element content was measured by ICP-OES (Agilent 725ES & Agilent 5110, Agilent Technologies, Santa Clara, CA, USA). The morphology and structure of materials

were recorded using scanning electron microscopy (Zeiss G300, Carl Zeiss Inc., Thornwood, New York, NY, USA) and transmission electron microscopy (JEOL Ltd., Tokyo, Japan). The elemental compositions and crystal structures of these samples were analyzed by X-ray photoelectron spectroscopy (XPS) (Thermo Scientific K-Alpha, Thermo Fisher Scientific, Waltham, MA, USA) and X-ray diffraction (Ultima IV, Rigaku Corporation, Tokyo, Japan).

2.3. Polysulfides Adsorption Experiment

Li_2S_6 solution with a concentration of 10 mmol L^{-1} was prepared by mixing lithium sulfide (Li_2S) and sulfur powder with a molar ratio of 1:5; the mixture was added into 1,3-dioxolane (DOL)/1,2-dimethoxyethane (DME) (1:1, *v/v*) solution, followed by intense stirring for 24 h in an Ar atmosphere. A total of 20 mg of TiN, Ta_2O_5 , and TiN/ Ta_2O_5 were added into 30 mL of Li_2S_6 solution, respectively, and rested for 12 h. The supernatant and precipitates were researched by UV-vis spectrophotometry and XPS.

2.4. Assembly of the Symmetric Cell

The electrode powers (TiN, Ta_2O_5 , and TiN/ Ta_2O_5), CNT, and polyvinylidene fluoride (PVDF) binder were dispersed into NMP with a weight ratio of 70:20:10 to form a homogeneous solution, and then it was coated onto the current collector. The symmetric cell used the electrodes as both cathode and anode, 30 μL electrolyte containing 0.5 mol L^{-1} of Li_2S_6 , and 1.0 mol L^{-1} of LiTFSI in a 1:1 (*v/v*) mixture of 1,3-dioxolane (DOL), and 1,2-dimethoxyethane (DME) was added into each coin cell. Cyclic voltammetry (CV) and electrochemical impedance spectroscopy (EIS) measurements were collected on an electrochemical workstation (VersaSTAT3, ametek, Berwyn, PA, USA).

2.5. Electrochemical Measurement

Standard CR2025 coin cells were assembled using the prepared electrodes and polypropylene separator (Celgard 2400, Celgard, Charlotte, NC, USA), with lithium metal as the anode. Charge-discharge performances of both coin cells and pouch cells were tested between 1.8 and 2.6 V using a LAND CT2001A (Landian, Wuhan, China) multi-channel battery testing system at room temperature.

In this experiment, the electrolyte was 1M LiTFSI in DOL/DME (1:1 *v/v*) containing LiNO_3 as an additive (1 wt%), The E/S ratio in the coin cells with areal sulfur loading (1.5 mg cm^{-2}) was controlled to be $10 \mu\text{L mg}^{-1}$. The pouch cells have average areal sulfur loading of 5.3 mg cm^{-2} and a decreased electrolyte/sulfur ratio of $3.3 \mu\text{L mg}^{-1}$.

3. Results and Discussion

The fabrication process of TiN@C/S/ Ta_2O_5 composite is shown in Figure 1. Firstly, Super P, CNT, graphene, and TiN were mixed and dispersed in deionized water to obtain the homogenous host materials. Sulfur was synthesized based on a disproportionated reaction. Then, the suspension of sulfur nanoparticles was added into the above host materials system. Through long-time stirring, all those materials were dispersed homogeneously without agglomeration, and the sulfur nanoparticles were evenly deposited in the TiN@C host. Finally, Ta(OEt)_5 was added to TiN@C/S slurry to shape the amorphous Ta_2O_5 by the hydrolysis reactions, which were well-dispersed on the external surface of TiN@C/S/ Ta_2O_5 .

Based on thermogravimetric analysis (TGA), the rationale design TiN@C/S/ Ta_2O_5 composite displays a sulfur content of 90 wt% in the sulfur composite (Figure 2a). Therefore, it is difficult for the low content 5% of both TiN and Ta_2O_5 to respond in X-raydiffractionpatterns (XRD) measurement (Ultima IV, Rigaku Corporation, Tokyo, Japan). The characteristic peaks of the TiN@C/S/ Ta_2O_5 composites are following the standard sulfur PDF card S (JCPDS 08-0247) (Figure S1), while the diffraction peaks of TiN and Ta_2O_5 can scarcely be found. To prove the existence of TiN and Ta_2O_5 , the TiN@C/S/ Ta_2O_5 composites were washed with carbon disulfide to wipe off redundant sulfur. TiN diffraction peaks, which are in accordance with the standard PDF card of TiN, and amorphous tantalum

oxide are discovered in the rinsed sample (Figure 2b). The mass ratio of Ta and Ti in TiN@C/S/Ta₂O₅ are 3.78 wt% and 3.52 wt% by ICP-OES testing. The surface chemical states of TiN@C/S/Ta₂O₅ were investigated by XPS under high vacuum, the display of strong peak intensity of Ta, and weak intensity Ti, further revealing the existence of an out-coated Ta₂O₅ layer in Figure 2c,d. The pore structures of the multidimensional carbon structure were studied using N₂ adsorption-desorption analysis. The BET-specified surface area of the multidimensional carbon structure was 352 m² g⁻¹. A dual distribution of micro-pore and mesopore was observed on the multidimensional carbon structure (Figure 2e,f); its electronic conductivity was 4.38×10^3 S m⁻¹.

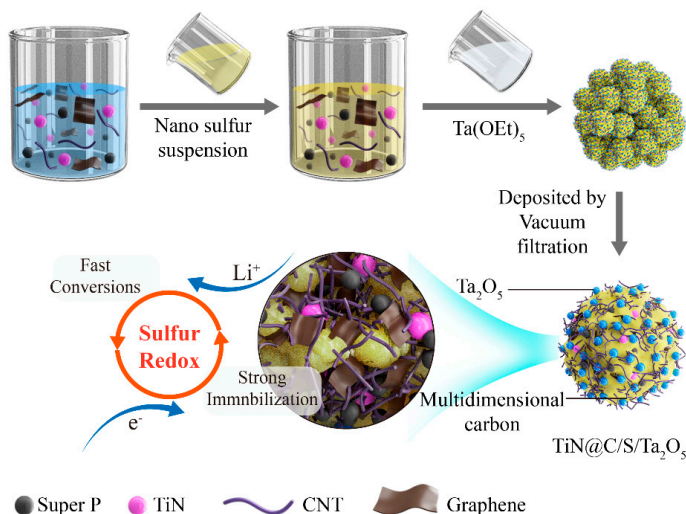


Figure 1. Schematic illustration of the synthesis route of the TiN@C/S/Ta₂O₅ composites.

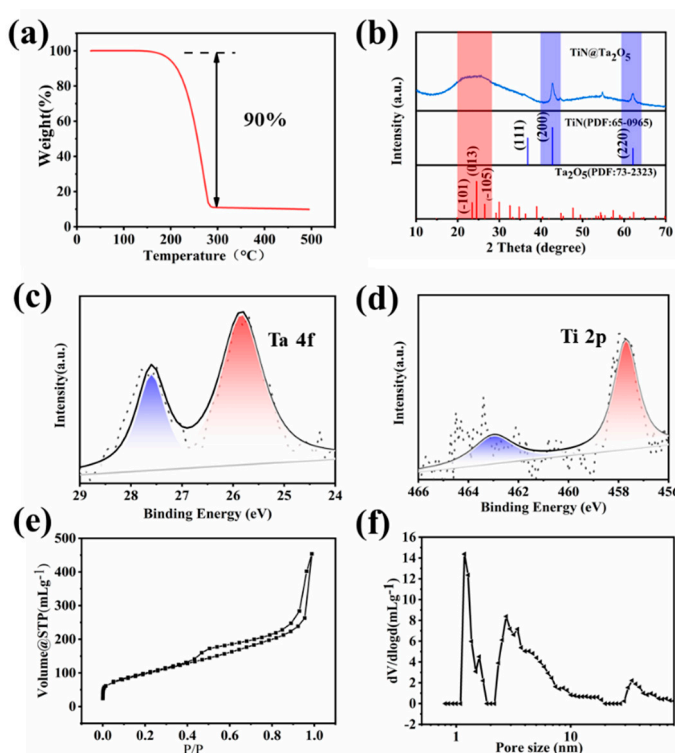


Figure 2. (a) TGA of TiN@C/S/Ta₂O₅ composites. (b) XRD patterns of TiN@C/Ta₂O₅ composites. (c,d) XPS spectra of TiN@C/S/Ta₂O₅ composites. (e) N₂ sorption isotherm and (f) pore size distribution based on QSDFT model of the multidimensional carbon structure.

The morphology of the TiN@C/S/Ta₂O₅ composites was investigated by scanning electron microscope (SEM); the TiN@C/S/Ta₂O₅ composite consists of a pile of clusters with an average size of about 0.2–1 µm (Figure 3a). The rough surface and hollow morphology guarantee the intimate contact between sulfur composites and electrolytes, leading to fast ion and electron transportation (Figure 3b).

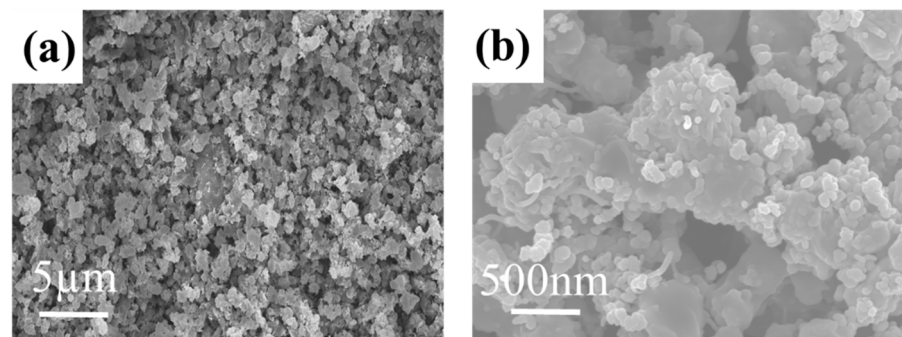


Figure 3. (a,b) SEM image of TiN@C/S/Ta₂O₅ composite.

The end products of the TiN@C/S/Ta₂O₅ composite electrode were displayed by transition electron microscope (TEM) observation. The closely packed nano-clusters structure is further conformed (Figure 4a). As displayed in the high-magnification TEM image (Figure 4b), the lattice spacings at 0.212 nm correspond to the (200) plane of TiN. Meanwhile, as shown in the (EDS) elemental mapping images in Figure 4c,g, Ti, N, Ta, O, and S elements are observed; these results manifest the formation of TiN@C/S/Ta₂O₅ composite. In addition, the EDS elemental mapping images of one single bulk TiN@C/S/Ta₂O₅ show that more signals of Ta and O can be observed, and most of them are on the surface of the unit; this result confirms the formation of the external Ta₂O₅ coating layer. Moreover, the existence of a few elements Ti and N imply that most TiN may be implanted inside the TiN@C/S/Ta₂O₅ composite (Figure S2).

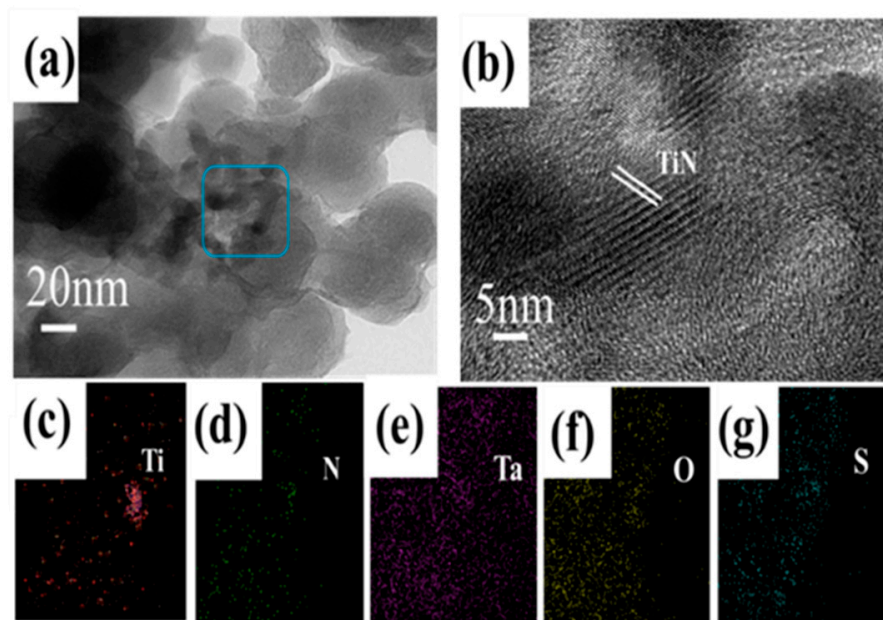


Figure 4. (a) TEM image of TiN@C/S/Ta₂O₅ material. (b) High-resolution TEM image of TiN@C/S/Ta₂O₅ material. (c–g) EDS elemental mapping images of TiN@C/S/Ta₂O₅ material with the selective regions shown in (a).

Polysulfides adsorption experiments were systematically implemented using the Li_2S_6 electrolyte for modeling polysulfide intermediates. In contrast, the Li_2S_6 solution turns almost transparent after being adsorbed by Ta_2O_5 and $\text{TiN}/\text{Ta}_2\text{O}_5$, while an obvious yellowish color still can be viewed for that with TiN . The absorbance was analyzed by UV-vis absorption spectra; it can be seen that the adsorption intensity with Ta_2O_5 and $\text{TiN}/\text{Ta}_2\text{O}_5$ solution decreases compared with others (Figure 5a). The X-ray photoelectron spectroscopy (XPS) technique was put into use to understand the chemical interaction of catalysts before and after the absorption of Li_2S_6 ; it can be observed that Ti 2p peaks have hardly any binding energy shift before and after the adsorption of Li_2S_6 (Figure 5b). However, the additional peak at 407.3 and 399.3 eV in the N 1 s spectrum of the Li_2S_6 -treated TiN corresponds to Ti-N-S bonding (Figure 5c), which should be ascribed to the electronegativity and polar of nitrogen; it ensures a strongly interaction with LiPSs and means that the exposed N sites are utilized as the main active sites for absorbing Li_2S_6 [20]. After interacting with Li_2S_6 , a large positive shift can be observed in both Ta 4f and O1s peaks in (Figure 5d,e); the shifts of these peak positions are considered to be produced by the strong binding interaction between Li_2S_6 and Ta_2O_5 , confirming their strong LiPSs adsorption capability [15].

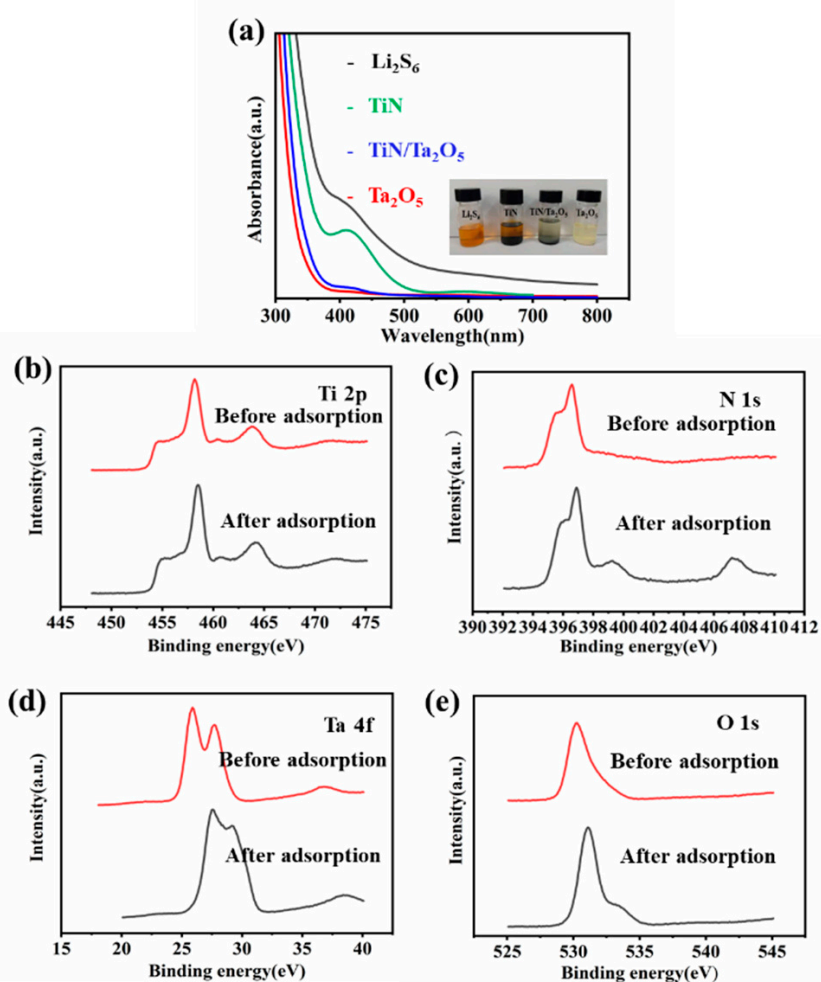


Figure 5. (a) UV-vis spectra of the Li_2S_6 solution with TiN , Ta_2O_5 , $\text{TiN}/\text{Ta}_2\text{O}_5$, and bare Li_2S_6 solution. (b–e) XPS spectra of Ti 2p, N 1s, Ta 4f, and O1s before and after adsorbed Li_2S_6 .

Symmetrical cells were assembled using TiN , Ta_2O_5 , and $\text{TiN}/\text{Ta}_2\text{O}_5$ identical electrodes and Li_2S_6 electrolyte to investigate the LiPSs conversion dynamics [21]. The $\text{TiN}/\text{Ta}_2\text{O}_5$ compound presents the strongest redox current peaks among different samples (Figure 6a), which could be attributed to the integrated adsorption and catalytic ability of

the TiN/Ta₂O₅ compound. Ta₂O₅ shows strong adsorption capability for polysulfides, but their intrinsically low electrical conductivity will impede the reaction kinetics of soluble LiPSs conversion into insoluble Li₂S/Li₂S₂. Similarly, although TiN exhibits good electrical conductivity, its weak affinities with lithium polysulfides cannot retain LiPSs to suppress the shuttling effect. Moreover, electrochemical impedance spectroscopy (EIS) analysis was employed to understand the interfacial charge transfer kinetics [22] (Figure 6b). TiN/Ta₂O₅ shows the smallest charge transfer resistance; the interface impedance of symmetric cells can explain the chemical affinity ability of the electrode materials to LiPSs and the ability of TiN/Ta₂O₅ to accept electrons when interacting with LiPSs, further reflecting its fast charge transfer and facile sulfur redox reactions at the TiN/Ta₂O₅ and polysulfides interface. All the above results reveal that the synergistic adsorptive-catalytic effect of TiN/Ta₂O₅ toward enhanced LiPSs conversions.

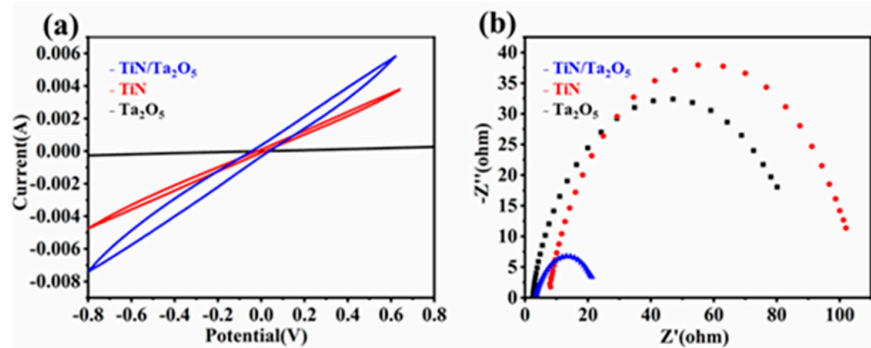


Figure 6. (a) CV curves of TiN, Ta₂O₅, and TiN/Ta₂O₅ symmetric cells with 0.1 M Li₂S₆ electrolyte. (b) EIS spectra of Li₂S₆ symmetrical cells.

To investigate the improved reaction kinetics of the TiN@C/S/Ta₂O₅ composites, the expedited polysulfides redox kinetics between solid-liquid-solid conversions was further indicated by the CV curves of the cells with TiN@C/S/Ta₂O₅, Ta₂O₅@C/S, and TiN@C/S electrodes at a scan rate of 0.1 mV s⁻¹ [23]. All the assembled cells show the typical pair of redox peaks. Compared with Ta₂O₅@C/S and TiN@C/S, CV curves of the TiN@C/S/Ta₂O₅ electrode display visibly stronger peak current intensity and closer peak position (Figure 7a). Additionally, the CV curves overlap well upon several cycles (Figure S3). At the same time, the voltage plateaus of galvanostatic charge/discharge profiles are also correspondent to peaks in the CV curves. The TiN@C/S/Ta₂O₅ cathode exhibits the highest specific capacity and a relatively lowest overpotential at 0.5C during the first cycle [24] (Figure 7b), when adsorptive-catalytic sites, both TiN and Ta₂O₅, were implanted within the multidimensional carbon structure. On the one hand, the dispersed-distribution Ta₂O₅ coating suggests stronger LiPSs adsorption capability due to the polar Ta-O bonding; it is found that long-chain polysulfides Li₂S₆ and Li₂S₈ are easily deformed after adsorbing on the surface of strong polar active sites Ta₂O₅. In this way, the Ta₂O₅ facilitates the fragmentation reactions of long-chain polysulfides into shorter chains and accelerates the kinetics of polysulfides conversion reactions by reducing the activation energy [25]. On the other hand, its high electrical conductivity of TiN can improve the reduction reaction kinetics by promoting electron transport in the electrode, resulting in rapid conversion of LiPSs into Li₂S. The TiN@C/S/Ta₂O₅ electrode owns the dual advantages of excellent trapping capability of LiPSs (Ta₂O₅) and superior electronic conductivity (TiN) to achieve the adsorption-catalysis synergy. The rate properties and corresponding charge-discharge profiles of these electrodes are displayed (Figure 7c and Figure S4); the TiN@C/S/Ta₂O₅ delivers the best rate performance with the highest discharge capacity of 1112 mAh g⁻¹ at 1C compared with Ta₂O₅@C/S (942 mAh g⁻¹) and TiN@C/S (993 mAh g⁻¹), the reversible capacity of 1216 mAh g⁻¹ when the current returns to 0.1 C. These results furtherly confirm the improved catalytic activity and kinetics for LiPSs conversion, which is due to the elaborate design of TiN@C/S/Ta₂O₅ composite. The charge/discharge voltage profiles of

TiN@C/S/Ta₂O₅ at various current densities are illustrated (Figure S4), TiN@C/S/Ta₂O₅ is capable of retaining the two-plateau discharge profile at a raised rate of up to 1 C without the severe electrochemical polarization-induced serious deformations of the voltage profile. The long-term cyclability performances are compared at a high current density of 0.5 C; the TiN@C/S/Ta₂O₅ cathode exhibits the optimal performances with an initial discharge capacity of 1175 mAh g⁻¹ at 0.5 C, which is much higher than all the other cathodes. The TiN@C/S/Ta₂O₅ cathode still delivers a decent discharge capacity of 660 mAh g⁻¹ and high Coulombic efficiency after 300 cycles (Figure 7d). The gentle capacity attenuation and prominent capacity retention of TiN@C/S/Ta₂O₅ cathode benefit from its abundant polysulfide-trapping and catalytic active sites: the out-coated Ta₂O₅ can serve as a covering layer to physically restrain part of LiPSs inside and chemically adsorb another part of out-diffused LiPSs on its polar active surface. Furthermore, TiN NPs presents satisfied catalysis ability to catalyze the conversion of LiPSs, originating from expediting electron transfer. With the synergistic and complementary roles of the cathode materials, the TiN@C/S/Ta₂O₅ cathode improves the efficient utilization of lithium polysulfides and promotes the chemical interaction with LiPSs and sulfur redox kinetics. It is worth noting that a distinct two-plateau discharge profile maintains well from the 1st to the 100 th cycle at a relatively high rate of 0.5 C (Figure S5), which is consistent with the results of cycling performance of TiN@C/S/Ta₂O₅ over 300 cycles at 0.5 C. This result is very competitive compared with the previously reported other electrodes (Table S1) [26–28] but it is under the condition of high S content up to 90 wt% and relatively low content of catalysts and carbon materials.

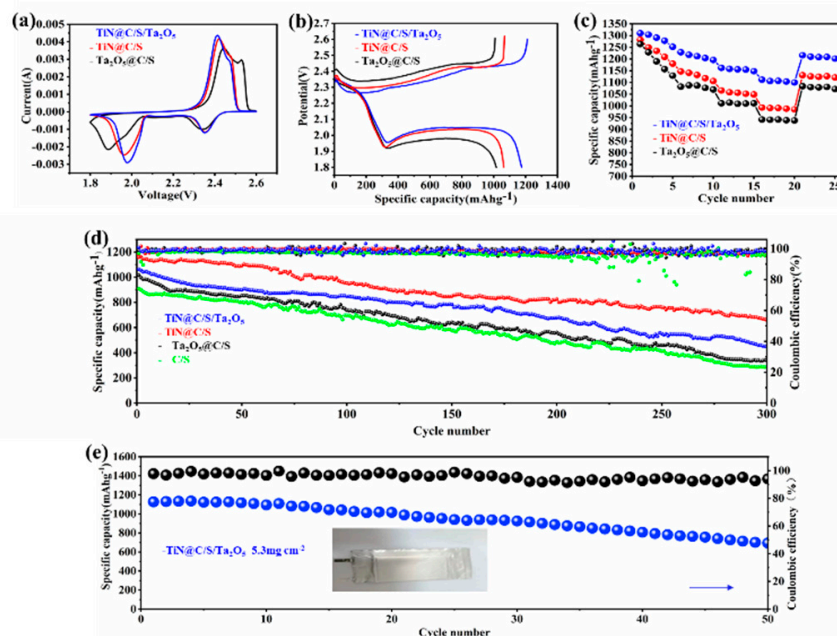


Figure 7. (a) CV curves of TiN@C/S/Ta₂O₅, Ta₂O₅@C/S, and TiN@C/S. (b) Galvanostatic charge-discharge curves of different cathodes at 0.5C. (c) rate performances of various sulfur electrodes. (d) Cycling performance of TiN@C/S/Ta₂O₅, Ta₂O₅@C/S, TiN@C/S and C/S cathodes at 0.5 C. (e) Cycling performances for TiN@C/Ta₂O₅/S pouch cells over 50 cycles at 0.2 C charge/discharge rate with a 5.3 mg cm⁻².

The wonderful performance of the TiN@C/S/Ta₂O₅ coin cell inspired us to fabricate a pouch cell with 200 mg sulfur loading in a single-piece cathode with dimensions of 75 mm × 50 mm. The pouch cell was cycled at a current density of 200 mA g⁻¹, the pouch cell showed a specific capacity of over 1100 mAh g⁻¹ with a capacity retention rate of 61.63% for 50 cycles (Figure 7e). Even the uniform Li metal corrosion caused by the dissolution and diffusion of LiPSs in the electrolyte could result in the fluctuation of Coulombic efficiency

with limited Li, but the pouch cell still shows high Coulombic efficiency of >96% and stable cycle life, further suggesting the function of the outer layer Ta_2O_5 in restraining the dissolution of LiPSs in organic electrolyte and eliminating Li metal corrosion. Our $TiN@C/S/Ta_2O_5$ pouch cell exhibits a superior electrocatalytic sulfur reduction reaction (SRR) and represents a significant advance in the light of specific capacity, good cycling life, and capacity retention when compared with some reported data (Table S2) [29–32]. Despite the substantial progress made in our work, there is much room to further enhance the energy densities by optimizing both the mass-production process and cell configuration for making the pouch cell.

4. Conclusions

In summary, the concept of combining the merits of rational materials to construct the high-energy-density lithium-sulfur battery has been introduced. The $TiN@C/S/Ta_2O_5$ composites with high sulfur fraction were synthesized via the co-precipitation method through a simple and low-cost preparation process. The novel design of $TiN@C/S/Ta_2O_5$ has demonstrated excellent cyclability and rate capability, owing to its potential for inhibiting the shuttle effect and facilitating LiPSs redox reaction in LSBs. Our work will guide the widespread commercialization of high-energy-density Li-S batteries.

Supplementary Materials: The following are available online at <https://www.mdpi.com/article/10.3390/nano1112882/s1>, Figure S1. XRD pattern of pure sulfur powder and $TiN@C/S/Ta_2O_5$ composite. Figure S2. EDS elemental mapping images of $TiN@C/S/Ta_2O_5$ material. Figure S3. CV profiles of $TiN@C/S/Ta_2O_5$ at a scan rate of 0.1 mV s^{-1} . Figure S4. Multi-rate discharge-charge profiles of $TiN@C/S/Ta_2O_5$. Figure S5. Discharge performance of $TiN@C/S/Ta_2O_5$ at different cycles at a rate of 0.5 C . Table S1. Performance Comparison with other sulfur electrodes. Table S2. Comparison of the pouch cell performance of our work with previously reported work focusing on sulfur cathodes.

Author Contributions: C.W.: design, analysis, investigation, writing—original draft. J.-H.L. and Z.-L.W.: software and investigation. A.-B.W. and H.Z.: investigation, methodology, formal analysis, and supervision. W.-K.W. and Z.-Q.J.: resources and supervision. L.-Z.F.: funding acquisition, resources, and supervision. All authors have read and agreed to the published version of the manuscript.

Funding: This research was supported by the National Natural Science Foundation of China (51872027) and the Beijing Natural Science Foundation (Z200011).

Conflicts of Interest: The authors declare no conflict of interest.

References

- Peng, H.J.; Huang, J.Q.; Cheng, X.B.; Zhang, Q. Review on High-Loading and High-Energy Lithium–Sulfur Batteries. *Adv. Energy Mater.* **2017**, *7*, 1700260. [[CrossRef](#)]
- Han, P.; Chung, S.H.; Manthiram, A. Recent Advances in Lithium Sulfide Cathode Materials and Their Use in Lithium Sulfur Batteries. *Energy Storage Mater.* **2019**, *17*, 317–324. [[CrossRef](#)]
- Liu, D.; Zhang, C.; Zhou, G.; Lv, W.; Ling, G.; Zhi, L.; Yang, Q.H. Catalytic Effects in Lithium-Sulfur Batteries: Promoted Sulfur Transformation and Reduced Shuttle Effect. *Adv. Sci.* **2018**, *5*, 1700270. [[CrossRef](#)]
- Xu, Z.L.; Lin, S.; Onofrio, N.; Zhou, L.; Shi, F.; Lu, W.; Kang, K.; Zhang, Q.; Lau, S.P. Exceptional catalytic effects of black phosphorus quantum dots in shuttling-free lithium sulfur batteries. *Nat. Commun.* **2018**, *9*, 4164. [[CrossRef](#)] [[PubMed](#)]
- Tsao, Y.; Lee, M.; Miller, E.C.; Gao, G.; Park, J.; Chen, S.; Katsumata, T.; Tran, H.; Wang, L.-W.; Toney, M.F. Designing a Quinone-Based Redox Mediator to Facilitate Li₂S Oxidation in Li-S Batteries. *Joule* **2019**, *3*, 872. [[CrossRef](#)]
- Pang, Q.; Kundu, D.P.; Cuisinier, M.; Nazar, L.F. Surface-enhanced redox chemistry of polysulphides on a metallic and polar host for lithium-sulphur batteries. *Nat. Commun.* **2014**, *5*, 4759. [[CrossRef](#)]
- Chao, D.; Zhu, C.; Yang, P.; Xia, X.; Liu, J.; Wang, J.; Fan, X.; Savilov, S.V.; Lin, J.; Fan, H.J.; et al. Array of nanosheets render ultrafast and high-capacity Na-ion storage by tunable pseudocapacitance. *Nat. Commun.* **2016**, *7*, 12122. [[CrossRef](#)]
- Sun, Z.H.; Zhang, J.Q.; Yin, L.C.; Hu, G.J.; Fang, R.P.; Cheng, H.M.; Li, F. Conductive porous vanadium nitride/graphene composite as chemical anchor of polysulfides for lithium-sulfur batteries. *Nat. Commun.* **2017**, *8*, 14627. [[CrossRef](#)]
- Chen, X.X.; Ding, X.Y.; Wang, C.S.; Feng, Z.Y.; Xu, L.Q.; Gao, X.; Zhai, Y.J.; Wang, D.B. A multi-shelled CoP nanosphere modified separator for highly efficient Li-S batteries. *Nanoscale* **2018**, *10*, 13694–13701. [[CrossRef](#)]

10. Xie, J.; Li, B.Q.; Peng, H.J.; Song, Y.W.; Zhao, M.; Chen, X.; Zhang, Q.; Huang, J.Q. Implanting Atomic Cobalt within Mesoporous Carbon toward Highly Stable Lithium-Sulfur Batteries. *Adv. Mater.* **2019**, *31*, 1903813. [[CrossRef](#)]
11. Zhou, T.H.; Lv, W.; Li, J.; Zhou, G.M.; Zhao, Y.; Fan, S.X.; Liu, B.L.; Li, B.H.; Kang, F.Y.; Yang, Q.H. Twinborn TiO_2 - TiN heterostructures enabling smooth trapping-diffusion-conversion of polysulfides towards ultralong life lithium-sulfur batteries. *Energy Environ. Sci.* **2017**, *10*, 16941703. [[CrossRef](#)]
12. Hao, Z.X.; Yuan, L.X.; Chen, C.J.; Xiang, J.W.; Li, Y.Y.; Huang, Z.M.; Hu, P.; Huang, Y.H. TiN as a simple and efficient polysulfide immobilizer for lithium-sulfur batteries. *J. Mater. Chem. A* **2016**, *4*, 17711–17717. [[CrossRef](#)]
13. Cui, Z.M.; Zu, C.X.; Zhou, W.D.; Manthiram, A.; Goodenough, J.B. Mesoporous Titanium Nitride-Enabled Highly Stable Lithium-Sulfur Batteries. *Adv. Mater.* **2016**, *28*, 6926–6931. [[CrossRef](#)] [[PubMed](#)]
14. Xing, Z.; Li, G.; Sy, S.; Chen, Z. Recessed deposition of TiN into N-doped carbon as a cathode host for superior Li-S batteries performance. *Nano Energy* **2018**, *54*, 1–9. [[CrossRef](#)]
15. Choi, J.; Jeong, T.G.; Lee, D.; Oh, S.H.; Jung, Y.; Kim, Y.T. Enhanced rate capability due to highly active Ta_2O_5 catalysts for lithium sulfur batteries. *J. Power Sources* **2019**, *435*, 226707. [[CrossRef](#)]
16. Zhang, Z.; Luo, D.; Li, G.; Gao, R.; Li, M.; Li, S.; Zhao, L.; Dou, H.; Wen, G.; Sy, S.; et al. Tantalum-Based Electrocatalyst for Polysulfide Catalysis and Retention for High-Performance Lithium-Sulfur Batteries. *Matter* **2020**, *3*, 920. [[CrossRef](#)]
17. Peng, H.J.; Huang, J.Q.; Zhao, M.Q.; Zhao, M.Q.; Zhang, Q.; Cheng, X.B.; Liu, X.Y.; Qian, W.Z.; Wei, F. Nanoarchitected Graphene/CNT@Porous Carbon with Extraordinary Electrical Conductivity and Interconnected Micro/Mesopores for Lithium-Sulfur Batteries. *Adv. Funct. Mater.* **2014**, *24*, 2772–2781. [[CrossRef](#)]
18. Xue, W.J.; Shi, Z.; Suo, L.M.; Wang, C.; Wang, Z.Q.; Wang, H.Z.; So, K.P.; Maurano, A.; Yu, D.W.; Chen, Y.M.; et al. Intercalation-conversion hybrid cathodes enabling Li-S full-cell architectures with jointly superior gravimetric and volumetric energy densities. *Nat. Energy* **2019**, *4*, 374–382. [[CrossRef](#)]
19. Li, Z.Q.; Xu, J.; Wang, J.; Niu, D.F.; Hu, S.Z.; Zhang, X.S. Well-dispersed Amorphous Ta_2O_5 Chemically Grafted onto Multi-Walled Carbon Nanotubes for High-performance Lithium Sulfur Battery. *Int. J. Electrochem. Sci.* **2019**, *14*, 6628–6642. [[CrossRef](#)]
20. Lim, W.G.; Jo, C.; Cho, A.; Hwang, J.; Kim, S.; Han, J.W.; Lee, J. Approaching Ultrastable High-Rate Li-S Batteries through Hierarchically Porous Titanium Nitride Synthesized by Multiscale Phase Separation. *Adv. Mater.* **2019**, *31*, 1806547. [[CrossRef](#)]
21. Shi, H.; Ren, X.; Lu, J.; Dong, C.; Liu, J.; Yang, Q.; Chen, J.; Wu, Z.-S. Dual-Functional Atomic Zinc Decorated Hollow Carbon Nanoreactors for Kinetically Accelerated Polysulfides Conversion and Dendrite Free Lithium Sulfur Batteries. *Adv. Energy Mater.* **2020**, *10*, 2002271. [[CrossRef](#)]
22. Shen, Z.; Cao, M.; Zhang, Z.; Pu, J.; Zhong, C.; Li, J.; Ma, H.; Li, F.; Zhu, J.; Pan, F.; et al. Efficient $Ni_2Co_4P_3$ Nanowires Catalysts Enhance Ultrahigh-Loading Lithium-Sulfur Conversion in a Microreactor-Like Battery. *Adv. Funct. Mater.* **2020**, *30*, 1906661. [[CrossRef](#)]
23. Chen, Y.; Choi, S.; Su, D.; Gao, X.; Wang, G. Self-standing sulfur cathodes enabled by 3D hierarchically porous titanium monoxide-graphene composite film for high-performance lithium-sulfur batteries. *Nano Energy* **2018**, *47*, 331. [[CrossRef](#)]
24. Li, Z.; Zhang, J.; Guan, B.; Wang, D.; Liu, L.M.; Lou, X.W. A sulfur host based on titanium monoxide@carbon hollow spheres for advanced lithium-sulfur batteries. *Nat. Commun.* **2016**, *7*, 13065. [[CrossRef](#)]
25. Wang, Y.; Huang, J.Y.; Lu, J.G.; Lu, B.; Ye, Z. Fabricating efficient polysulfide barrier via ultrathin tantalum pentoxide grown on separator for lithium-sulfur batteries. *J. Electroanal. Chem.* **2019**, *854*, 113539. [[CrossRef](#)]
26. Su, D.; Cortie, M.; Fan, H.; Wang, G. Prussian Blue Nanocubes with an Open Framework Structure Coated with PEDOT as High-Capacity Cathodes for Lithium-Sulfur Batteries. *Adv. Mater.* **2017**, *29*, 1700587. [[CrossRef](#)] [[PubMed](#)]
27. Bao, W.; Su, D.; Zhang, W.; Guo, X.; Wang, G. 3D Metal Carbide@Mesoporous Carbon Hybrid Architecture as a New Polysulfide Reservoir for Lithium-Sulfur Batteries. *Adv. Funct. Mater.* **2016**, *26*, 8746–8756. [[CrossRef](#)]
28. Sun, Q.; Xi, B.; Li, J.-Y.; Mao, H.; Ma, X.; Liang, J.; Feng, J.; Xiong, S. Nitrogen-Doped Graphene-Supported Mixed Transition-Metal Oxide Porous Particles to Confine Polysulfides for Lithium-Sulfur Batteries. *Adv. Energy Mater.* **2018**, *8*, 1800595. [[CrossRef](#)]
29. Luo, L.; Li, J.; Asl, H.Y.; Manthiram, A. *In-Situ* Assembled VS₄ as a Polysulfide Mediator for High-Loading Lithium-Sulfur Batteries. *ACS Energy Lett.* **2020**, *5*, 1177–1185. [[CrossRef](#)]
30. Luo, L.; Chung, S.H.; Asl, H.Y.; Manthiram, A. Long-Life Lithium-Sulfur Batteries with a Bifunctional Cathode Substrate Configured with Boron Carbide Nanowires. *Adv. Mater.* **2018**, *30*, 1804149. [[CrossRef](#)] [[PubMed](#)]
31. Kim, M.S.; Kim, M.S.; Do, V.D.; Xia, Y.Y.; Kim, W.; Cho, W. Facile and scalable fabrication of high-energy-density sulfur cathodes for pragmatic lithium-sulfur batteries. *J. Power Sources* **2019**, *422*, 104–112. [[CrossRef](#)]
32. Zhang, J.; You, C.; Wang, J.; Xu, H.; Zhu, C.; Guo, S.; Zhang, W.; Yang, R.; Xu, Y. Confinement of sulfur species into heteroatom-doped, porous carbon container for high areal capacity cathode. *Chem. Eng. J.* **2019**, *368*, 340–349. [[CrossRef](#)]